

# Role of NH<sub>3</sub> in the Dehydrogenation of Calcium Amidoborane Ammoniate and Magnesium Amidoborane Ammoniate: A First-Principles Study

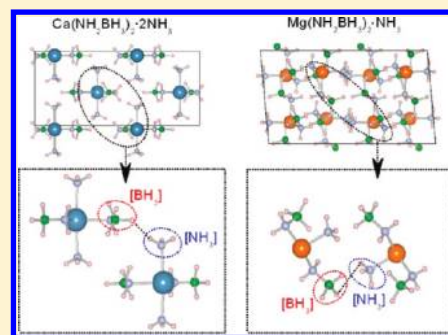
Wen Li,<sup>†,‡</sup> Guotao Wu,<sup>†</sup> Yongshen Chua,<sup>†,§</sup> Yuan Ping Feng,<sup>‡</sup> and Ping Chen<sup>\*,†</sup>

<sup>†</sup>Dalian Institute of Chemical Physics, Chinese Academy of Sciences, Dalian 116023, P.R. China

<sup>‡</sup>Department of Physics and <sup>§</sup>Department of Chemistry, National University of Singapore, 117542, Singapore

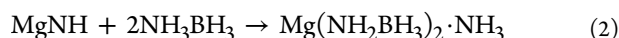
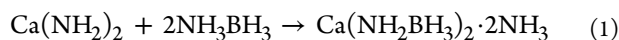
## S Supporting Information

**ABSTRACT:** First-principles calculations show that [NH<sub>3</sub>] molecules play crucial roles as both activator for the break-up of B–H bond and supplier of protic H for the establishment of dihydrogen bonding, which could facilitate the dehydrogenation of Ca(NH<sub>2</sub>BH<sub>3</sub>)<sub>2</sub>·2NH<sub>3</sub> or Mg(NH<sub>2</sub>BH<sub>3</sub>)<sub>2</sub>·NH<sub>3</sub> occurring at lower temperatures compared to those of Ca(NH<sub>2</sub>BH<sub>3</sub>)<sub>2</sub> and Mg(NH<sub>2</sub>BH<sub>3</sub>)<sub>2</sub>. Moreover, the calculations of Helmholtz Free energy and [NH<sub>3</sub>] molecule removal energy evidence that coordination between [NH<sub>3</sub>] and Mg cation is stronger than that between [NH<sub>3</sub>] and Ca cation; therefore, Mg(NH<sub>2</sub>BH<sub>3</sub>)<sub>2</sub>·NH<sub>3</sub> will undergo directly dehydrogenation rather than deammoniation at lower temperatures.



## 1. INTRODUCTION

Ammonia borane (NH<sub>3</sub>BH<sub>3</sub>) has been being actively pursued for hydrogen storage because of its high gravimetric hydrogen capacity of 19.6 wt %;<sup>1</sup> however, it suffers from a few drawbacks such as the slow kinetics and unfavorable thermodynamics of dehydrogenation, which limits its practical application in polymer electrolyte membrane (PEM) fuel cells.<sup>2–4</sup> A series of chemical hydride systems derived from NH<sub>3</sub>BH<sub>3</sub> have been recently developed to improve the dehydrogenation properties of NH<sub>3</sub>BH<sub>3</sub>. For example, substituting one H atom in the [NH<sub>3</sub>] group in NH<sub>3</sub>BH<sub>3</sub> by an alkali metal or alkaline earth metal element leads to the formation of metal amidoboranes such as lithium amidoborane (LiNH<sub>2</sub>BH<sub>3</sub>),<sup>5–10</sup> sodium amidoborane (NaNH<sub>2</sub>BH<sub>3</sub>),<sup>6,10,11</sup> or calcium amidoborane (Ca(NH<sub>2</sub>BH<sub>3</sub>)<sub>2</sub>), abbreviated in the following as CaAB.<sup>12</sup> More recently, amidoborane ammoniates, a new sort of chemical hydride system including calcium amidoborane ammoniate (Ca(NH<sub>2</sub>BH<sub>3</sub>)<sub>2</sub>·2NH<sub>3</sub>), abbreviated in the following as CaAB·2NH<sub>3</sub>,<sup>13</sup> magnesium amidoborane monoammoniate (Mg(NH<sub>2</sub>BH<sub>3</sub>)<sub>2</sub>·NH<sub>3</sub>), abbreviated in the following as MgAB·NH<sub>3</sub>,<sup>14</sup> and lithium amidoborane ammoniate (Li(NH<sub>3</sub>)NH<sub>2</sub>BH<sub>3</sub>), abbreviated in the following as LiAB·NH<sub>3</sub>,<sup>15</sup> have been synthesized by reacting metal amidoborane and ammonia or metal amide/imide and ammonia borane,



It was shown experimentally that those ammoniates released hydrogen at lower temperatures compared to the H-desorption

temperatures of the corresponding metal amidoboranes.<sup>13,15,16</sup> In a closed system, the dehydrogenation of CaAB·2NH<sub>3</sub> starts at ~343 K, and releases ~8.2 wt % H<sub>2</sub> upon heating at 423 K,<sup>13</sup> which shows significant advantages over CaAB (starting to release H<sub>2</sub> at ~403 K, peaking at 423 K).<sup>8</sup> MgAB·NH<sub>3</sub> desorbs hydrogen at ~323 K with vigorous hydrogen release at 347 K, while MgAB was found unstable at ambient temperature.<sup>16</sup> LiAB·NH<sub>3</sub> releases hydrogen at temperature above 313 K, in particular, under ammonia, LiAB·NH<sub>3</sub> provides a high hydrogen storage capacity (11.18 wt % H<sub>2</sub>) at the easily accessible dehydrogenation temperature of 333 K, which shows more favorable performance than LiAB (releasing hydrogen at ~363 K).<sup>15</sup>

Recent theoretical studies on alkali and alkaline earth metal amidoboranes revealed that the metal element acts as electron donor to N, leading to the alteration of the bond nature and strength and charge density distributions.<sup>8,17</sup> The results from gas-phase simulations indicated that a hydrogen of [BH<sub>3</sub>] transfers to the metal cation forming a metal hydride intermediate, and the metal hydride acts as a hydridic source for the dehydrogenation, which facilitates H<sub>2</sub> to release at a lower kinetic barrier.<sup>18,19</sup> As a consequence, reduced dehydrogenation temperatures are achieved in metal amidoboranes compared to that of neat ammonia borane. Those studies on alkali and alkaline earth metal amidoboranes provide general insight into the dehydrogenation mechanism for the metal–B–N–H containing chemical hydrides, that is, the dihydrogen interaction between hydridic H(B) and protic H(N), and subsequent detachment and combination of H(B) and H(N)

Received: May 11, 2011

Published: December 12, 2011



atoms. In metal amidoborane ammoniates, the coordinated  $[\text{NH}_3]$  molecules in the lattice could provide additional protic  $\text{H}(\text{N})$  to interact with hydridic  $\text{H}(\text{B})$ . Moreover, the coordination between the  $[\text{NH}_3]$  molecule and the metal cation may alter the interaction between cation and amidoborane anion, which further affects  $\text{B}-\text{H}$  and  $\text{N}-\text{H}$  bonds; as a consequence, the detachment and combination of  $\text{H}(\text{B})$  and  $\text{H}(\text{N})$  atoms were observed to occur at lower temperatures.<sup>13</sup>

To understand the dehydrogenation mechanism of metal amidoborane ammoniates and to examine the role of  $[\text{NH}_3]$  molecule during the dehydrogenation, in this paper, we employed first-principles calculations based on density functional theory (DFT) to investigate the electronic and phononic structures, hydrogen desorption and diffusion, and the thermodynamics of deammoniation in solid  $\text{CaAB}$ ,  $\text{CaAB}\cdot 2\text{NH}_3$ ,  $\text{MgAB}$ , and  $\text{MgAB}\cdot \text{NH}_3$ . Our results show that the  $[\text{NH}_3]$  molecule in metal amidoborane ammoniates plays a crucial role as both activator of the break-up of the hydridic  $\text{B}-\text{H}$  bond and supplier of protic  $\text{H}$  for the establishment of dihydrogen bonding, which could facilitate lower dehydrogenation temperatures of metal amidoborane ammoniates compared to those of metal amidoboranes. The first-step dehydrogenation was identified to be the dissociation of a  $\text{H}(\text{B})$  atom from the  $[\text{NH}_2\text{BH}_3]$  anion and a  $\text{H}(\text{N})$  atom from nearby  $[\text{NH}_3]$  molecule, and subsequent combination of  $\text{H}(\text{B})$  and  $\text{H}(\text{N})$  to form  $\text{H}_2$ . Furthermore, we tentatively simulated the hydrogen diffusion process in  $\text{CaAB}$ ,  $\text{CaAB}\cdot 2\text{NH}_3$ , and  $\text{MgAB}\cdot \text{NH}_3$  and found that the hydrogen migration energy may contribute to the activation energy to be overcome in the initiation of dehydrogenation. The deammoniation thermodynamics of  $\text{CaAB}\cdot 2\text{NH}_3$  and  $\text{MgAB}\cdot \text{NH}_3$  derived from finite-temperature phonon calculations suggested that deammoniation of  $\text{MgAB}\cdot \text{NH}_3$  is only thermodynamically allowed above 373 K, which explains why ammonia gas is hardly detected experimentally at lower temperatures in the decomposition of  $\text{MgAB}\cdot \text{NH}_3$ . Finally, the investigation of the coordination strength between metal cation and  $[\text{NH}_3]$  molecules in  $\text{CaAB}\cdot 2\text{NH}_3$  and  $\text{MgAB}\cdot \text{NH}_3$  revealed that  $[\text{NH}_3]$  molecules are more strongly coordinated with the  $\text{Mg}$  cation, allowing  $\text{MgAB}\cdot \text{NH}_3$  to release  $\text{H}_2$  rather than  $\text{NH}_3$  at lower temperatures.

## 2. THEORETICAL CALCULATIONS

**2.1. First-Principles Calculations.** First-principles calculations were carried out within the framework of DFT<sup>20</sup> using the projector-augmented wave (PAW) method<sup>21</sup> as implemented in the Vienna Ab initio Simulation Package (VASP) code.<sup>22</sup> Electronic exchange and correlations treated by the generalized gradient approximation (GGA)<sup>23</sup> of Perdew and Wang 1991 (PW91)<sup>24,25</sup> are widely employed for the first-principles calculations of metal-B-N-H based hydrogen storage materials,<sup>26–29</sup> as it is proven to be generally more reliable than the local density approximation (LDA) for the energetic problems. We computed the structural properties of  $\text{CaAB}$ ,  $\text{CaAB}\cdot 2\text{NH}_3$ ,  $\text{MgAB}$ , and  $\text{MgAB}\cdot \text{NH}_3$  by using GGA of PW91, GGA of Perdew–Burke–Ernzerhof (PBE),<sup>30</sup> and LDA, respectively. A comparison of calculated results and the experimental data are listed in the Supporting Information, Table S1, indicating that GGA calculations are significantly closer to experiment than LDA. The calculated lattice parameters and detailed atomic positions using GGA-PW91 are listed in Supporting Information, Table S2.

$\text{CaAB}$  has a monoclinic structure (space group  $\text{C}2$ , No.5),<sup>31</sup> and  $\text{CaAB}\cdot 2\text{NH}_3$  crystallizes into orthorhombic (space group  $\text{Pna}2_1$ , No.33).<sup>13</sup>  $\text{MgAB}$  cannot crystallize at room temperature. Generally, the metal amidoboranes with the metal cation in the same group of

elements are isostructural, for example,  $\text{LiAB}$  and  $\text{NaAB}$ ,  $\text{CaAB}$  and  $\text{SrAB}$ , therefore it is reasonable to expect that  $\text{MgAB}$  and  $\text{CaAB}$  are also isostructural. So we construct the crystal structure of  $\text{MgAB}$  by substituting  $\text{Ca}$  with  $\text{Mg}$  in  $\text{CaAB}$ . The structure of  $\text{MgAB}\cdot \text{NH}_3$  belongs to monoclinic (space group  $\text{P}2_1/\text{c}$ , No.14).<sup>16</sup> Full geometry optimization without any constraint was done by minimizing the Hellmann–Feynman forces on the atoms and stresses on the unit cell. For the static energy calculations, the self-consistency was achieved with a tolerance in total energy of 0.01 meV, atomic forces were converged to be less than 0.01 eV/Å. The electronic density of states (DOS) were calculated by means of the tetrahedron method with Blöchl corrections.<sup>32</sup> The  $1 \times 2 \times 2$ ,  $1 \times 2 \times 1$ ,  $1 \times 2 \times 2$ , and  $1 \times 1 \times 2$  supercells of  $\text{CaAB}$ ,  $\text{CaAB}\cdot 2\text{NH}_3$ ,  $\text{MgAB}$ , and  $\text{MgAB}\cdot \text{NH}_3$  were employed, respectively, in the consequent static calculations by using an energy cutoff of 520 eV and  $4 \times 4 \times 4$   $k$ -point meshes generated in the Monkhorst–Pack scheme.<sup>33</sup> The molecule of  $\text{NH}_3$  was calculated in a cubic box with edge of  $15 \times 15 \times 15 \text{ Å}^3$  to eliminate the interaction between molecules caused by periodic boundary conditions.

**2.2. Phonon Calculations.** The phonon DOS and reaction enthalpy were calculated using the direct method,<sup>34,35</sup> which was implemented in the Phonopy program<sup>36</sup> combined with VASP code. Hellmann–Feynman forces on all atoms in the supercell were calculated with the displacements of 0.03 Å for each symmetrically nonequivalent atom from their respective equilibrium positions in three independent directions. A complete force-constant matrix was obtained, and the phonon frequencies ( $\omega$ ) were then calculated by a diagonalization of the dynamical matrix. The  $1 \times 2 \times 2$  supercells of crystal  $\text{CaAB}$  and  $\text{MgAB}$ , a  $1 \times 3 \times 2$  supercell of  $\text{CaAB}\cdot 2\text{NH}_3$ , and a  $2 \times 2 \times 2$  supercell of  $\text{MgAB}\cdot \text{NH}_3$  were employed for the phonon calculations. For the gaseous  $\text{NH}_3$  molecule,  $2 \times 2 \times 2$  supercell has been chosen for phonon calculations. The PAW GGA potentials, cutoff energies, and the self-consistent field convergence parameters were chosen to be the same as for the static energy calculations described above, while atomic forces were converged to be lower than 0.001 eV/Å.

**2.3. Nudged Elastic Band (NEB) Method.** To determine the diffusion pathways and migration energy barriers of hydrogen atom in solid  $\text{CaAB}$ ,  $\text{CaAB}\cdot 2\text{NH}_3$ , and  $\text{MgAB}\cdot \text{NH}_3$ , we used the nudged elastic band (NEB) method,<sup>37</sup> which is implemented in VASP code. The intermediate images were generated in the computation, and each image was relaxed until the maximum residual force was less than 0.01 eV/Å.

## 3. RESULTS AND DISCUSSION

**3.1. Geometry.** Figure 1 shows the supercells of solid  $\text{CaAB}$ ,  $\text{CaAB}\cdot 2\text{NH}_3$ ,  $\text{MgAB}$ , and  $\text{MgAB}\cdot \text{NH}_3$ . The selected bond angles information in each structure is summarized in Table 1. The structure of  $\text{CaAB}$  consists of  $[\text{Ca}(\text{NH}_2\text{BH}_3)_2]$  molecule layers perpendicular to the  $[010]$  direction. In one  $[\text{Ca}(\text{NH}_2\text{BH}_3)_2]$  molecule, each  $\text{Ca}$  cation coordinates with two symmetrically equivalent  $[\text{NH}_2\text{BH}_3]$  anions (denoted as  $[\text{AB}]_{\text{I}}$ ), with the bond angle  $\angle \text{N}_{[\text{AB}](1)}-\text{Ca}-\text{N}_{[\text{AB}](2)}$  of  $161.37^\circ$ , and the  $\text{Ca}$ ,  $\text{N}$ , and  $\text{B}$  atoms are almost aligned in the same  $(010)$  plane. The  $\text{Ca}$  cation in  $\text{CaAB}\cdot 2\text{NH}_3$  coordinates with two symmetrically nonequivalent  $[\text{NH}_2\text{BH}_3]$  anions (denoted as  $[\text{AB}](1)_{\text{II}}$  and  $[\text{AB}](2)_{\text{II}}$ ) and two symmetrically nonequivalent  $[\text{NH}_3]$  molecules (denoted as  $\text{NH}_3(1)_{\text{II}}$  and  $\text{NH}_3(2)_{\text{II}}$ ), with the bond angles  $\angle \text{N}_{[\text{AB}](1)}-\text{Ca}-\text{N}_{[\text{AB}](2)}$  of  $105.67^\circ$  and  $\angle \text{N}_{[\text{NH}_3](1)}-\text{Ca}-\text{N}_{[\text{NH}_3](2)}$  of  $170.61^\circ$  ( $\text{N}_{[\text{AB}]}$  and  $\text{N}_{[\text{NH}_3]}$  denote the  $\text{N}$  atom located in the  $[\text{AB}]$  anion and  $[\text{NH}_3]$  molecule, respectively). The bridging bond of  $\text{B}-\text{N}_{[\text{AB}](1)}-\text{Ca}-\text{N}_{[\text{AB}](2)}-\text{B}$  lies in the direction parallel to the  $(001)$  plane, which is almost perpendicular to the bridging bond of  $\text{N}_{[\text{NH}_3](1)}-\text{Ca}-\text{N}_{[\text{NH}_3](2)}$ . Similar to  $\text{CaAB}$ , each  $\text{Mg}$  cation coordinates with two symmetrically equivalent  $[\text{NH}_2\text{BH}_3]$  anions (denoted as  $[\text{AB}]_{\text{III}}$ ) in  $\text{MgAB}$ , with the

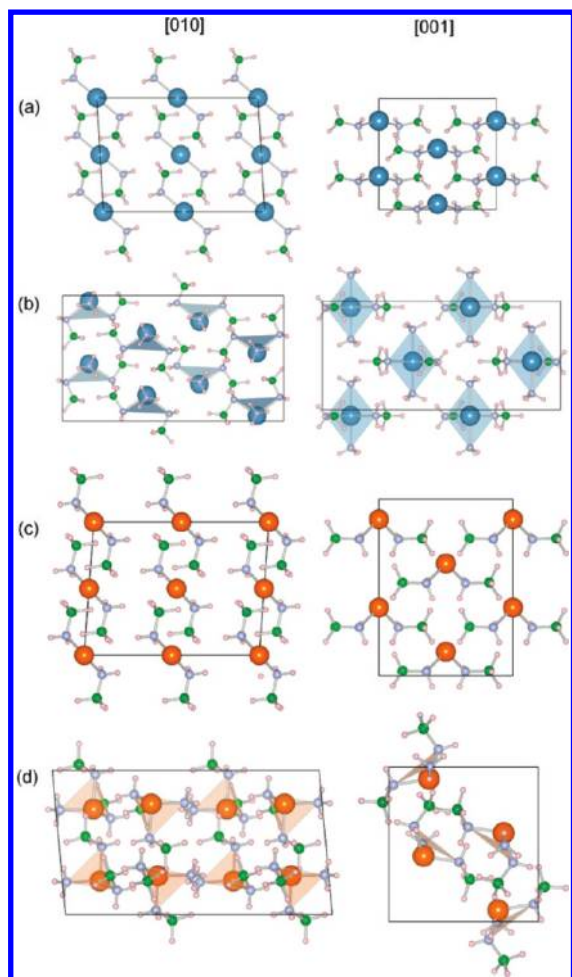


**Figure 1.** Crystal structure of (a)  $\text{Ca}(\text{NH}_2\text{BH}_3)_2$ , (b)  $\text{Ca}(\text{NH}_2\text{BH}_3)_2 \cdot 2\text{NH}_3$ , (c)  $\text{Mg}(\text{NH}_2\text{BH}_3)_2$ , and (d)  $\text{Mg}(\text{NH}_2\text{BH}_3)_2 \cdot \text{NH}_3$ . The structures are shown in a bond-stick view, and the viewing directions shown are all along the [010] (left panels) and [001] (right panels) direction. The large blue, large orange, small light blue, small green, small pink spheres denote Ca, Mg, N, B, and H atom, respectively.

bond angle  $\angle \text{N}_{[\text{AB}](1)}\text{--Mg--N}_{[\text{AB}](2)}$  of  $106.90^\circ$ . In  $\text{MgAB} \cdot \text{NH}_3$ , each Mg cation is coordinated in two symmetrically non-equivalent  $[\text{NH}_2\text{BH}_3]$  anions (denoted as  $[\text{AB}](1)_{\text{IV}}$  and  $[\text{AB}](2)_{\text{IV}}$ ) and a single  $[\text{NH}_3]$  molecule, and Mg is located at the top of nitrogen triangle plane formed by two  $\text{N}_{[\text{AB}]}$  atoms and one  $\text{N}_{[\text{NH}_3]}$  atom. The bond angles of  $\angle \text{N}_{[\text{AB}](1)}\text{--Mg--N}_{[\text{AB}](2)}$ ,  $\angle \text{N}_{[\text{AB}](1)}\text{--Mg--N}_{[\text{NH}_3]}$ , and  $\angle \text{N}_{[\text{AB}](2)}\text{--Mg--N}_{[\text{NH}_3]}$  are  $100.50^\circ$ ,  $97.63^\circ$ , and  $111.81^\circ$ , respectively. The  $\text{Mg--N}_{[\text{NH}_3]}$  bond points to the direction of the  $c$ -axis.

**3.2. Electronic DOS.** The calculated total and partial electronic DOS for CaAB, CaAB·2NH<sub>3</sub>, MgAB, and

MgAB·NH<sub>3</sub> are shown in Figure 2. In general, they have finite energy gaps between valence bands and conduction bands and therefore exhibit nonmetallic features. The calculated GGA band gaps of CaAB and CaAB·2NH<sub>3</sub> ( $\sim 4$  eV) are lightly narrower than those of MgAB and MgAB·NH<sub>3</sub> ( $\sim 5$  eV). The actual gap could be even larger since DFT is known to underestimate the band gap of semiconductors and insulators. The covalent feature of B–N, N–H, and B–H bonds is clearly indicated by the strong  $sp$  hybridization of states between B and N, N and H(N), B and H(B) atoms within the valence band region. The interaction between Ca/Mg cation and  $[\text{NH}_2\text{BH}_3]$  anion is essentially ionic, which is identified by the broad peaks of Ca/Mg  $s$ - and  $p$ -states in the conduction band region. The coordination interaction between Ca/Mg cation and  $[\text{NH}_3]$  molecule is mainly covalent because of the overlapping electron densities of  $\text{N}_{[\text{NH}_3]}$   $p$ -states and Ca/Mg  $s$ - and  $p$ -states in the valence band region.

**3.3. Phonon DOS.** To establish finite-temperature properties, we calculated the phonons for all systems. Figure 3 displays the total and atom-decomposed phonon DOS derived from the calculated phonon spectra of CaAB, CaAB·2NH<sub>3</sub>, MgAB, and MgAB·NH<sub>3</sub>. The vibrational spectra of these systems can be generally classified into several segments defined by the molecular feature from high-frequency to low-frequency region as follows: the N–H stretching mode ( $3300\text{--}3500\text{ cm}^{-1}$ ), the B–H stretching mode (around  $2250\text{ cm}^{-1}$ ),  $\text{NH}_3$  ( $1625\text{ cm}^{-1}$ ) or  $\text{NH}_2$  ( $1550\text{ cm}^{-1}$ ) deformation mode,  $\text{BH}_3$  deformation mode ( $1110\text{--}1250\text{ cm}^{-1}$ ), B–N stretching mode (around  $900\text{ cm}^{-1}$ ), N–H and B–H rocking modes ( $750\text{--}900\text{ cm}^{-1}$ ), Ca/Mg translational lattice mode and Ca/Mg–N rotational mode (below  $350\text{ cm}^{-1}$ ). The spectrum of CaAB·2NH<sub>3</sub> matches well with the experimental observation by Fourier transform infrared (FTIR) spectroscopy, in which  $3000\text{--}3400\text{ cm}^{-1}$  is for N–H stretching,  $2150\text{--}2270\text{ cm}^{-1}$  for B–H stretching, and  $600\text{--}1000\text{ cm}^{-1}$  for B–N stretching.<sup>13</sup> N–H stretching consists of two dominant peaks above  $3250\text{ cm}^{-1}$ . It is noted that subtle downshifts in the peak position are observed for N–H bond-stretching mode in the  $[\text{NH}_3]$  molecule compared to that in the  $[\text{AB}]$  anion in the partial phonon DOS of CaAB·2NH<sub>3</sub> and MgAB·NH<sub>3</sub>. B–H stretching is associated with two dominant peaks and one shoulder peak in the lower frequency region around  $2250\text{ cm}^{-1}$ . The above results could indicate the strength of N–H and B–H bonds is in the order of:  $\text{N--H}_{[\text{NH}_3]} < \text{N--H}_{[\text{AB}]} < \text{B--H}_{[\text{AB}]}$ , which will be confirmed by the analyses of bond lengths below.

**3.4. Chemical Bond Lengths.** The selected atomic distances in all systems are summarized in Table 2. The bond lengths in symmetrically nonequivalent groups and molecules are examined separately. The distance of  $\text{Ca}_{\text{I}} \cdots \text{H}(\text{B})_{\text{I}}$  between Ca cation and nearby hydridic H(B) atom in CaAB is  $2.363\text{ \AA}$ , shorter than the  $\text{Ca}_{\text{II}} \cdots \text{H}(\text{B})_{\text{II}}$  distance of  $2.421\text{ \AA}$  in CaAB·2NH<sub>3</sub>. The B–N bond length of  $1.546\text{ \AA}$  in the  $[\text{AB}]_{\text{I}}$

**Table 1.** Calculated Bond Angles (deg) in  $\text{Ca}(\text{NH}_2\text{BH}_3)_2$  (CaAB),  $\text{Ca}(\text{NH}_2\text{BH}_3)_2 \cdot 2\text{NH}_3$  (CaAB·2NH<sub>3</sub>),  $\text{Mg}(\text{NH}_2\text{BH}_3)_2$  (MgAB), and  $\text{Mg}(\text{NH}_2\text{BH}_3)_2 \cdot \text{NH}_3$  (MgAB·NH<sub>3</sub>)

	CaAB	CaAB·2NH <sub>3</sub>	MgAB	MgAB·NH <sub>3</sub>
$\angle \text{N}_{[\text{AB}](1)}\text{--Ca/Mg--N}_{[\text{AB}](2)}^a$	161.37	105.67	106.90	100.50
$\angle \text{N}_{[\text{NH}_3](1)}\text{--Ca/Mg--N}_{[\text{NH}_3](2)}$		170.61		
$\angle \text{N}_{[\text{AB}](1)}\text{--Ca/Mg--N}_{[\text{NH}_3]}$		86.72/87.46		97.63
$\angle \text{N}_{[\text{AB}](2)}\text{--Ca/Mg--N}_{[\text{NH}_3]}$		88.07/86.41		111.81

<sup>a</sup>The numbers (1) and (2) in the parentheses denote two  $[\text{AB}]$  anions or  $[\text{NH}_3]$  molecules coordinated with Ca/Mg cation.



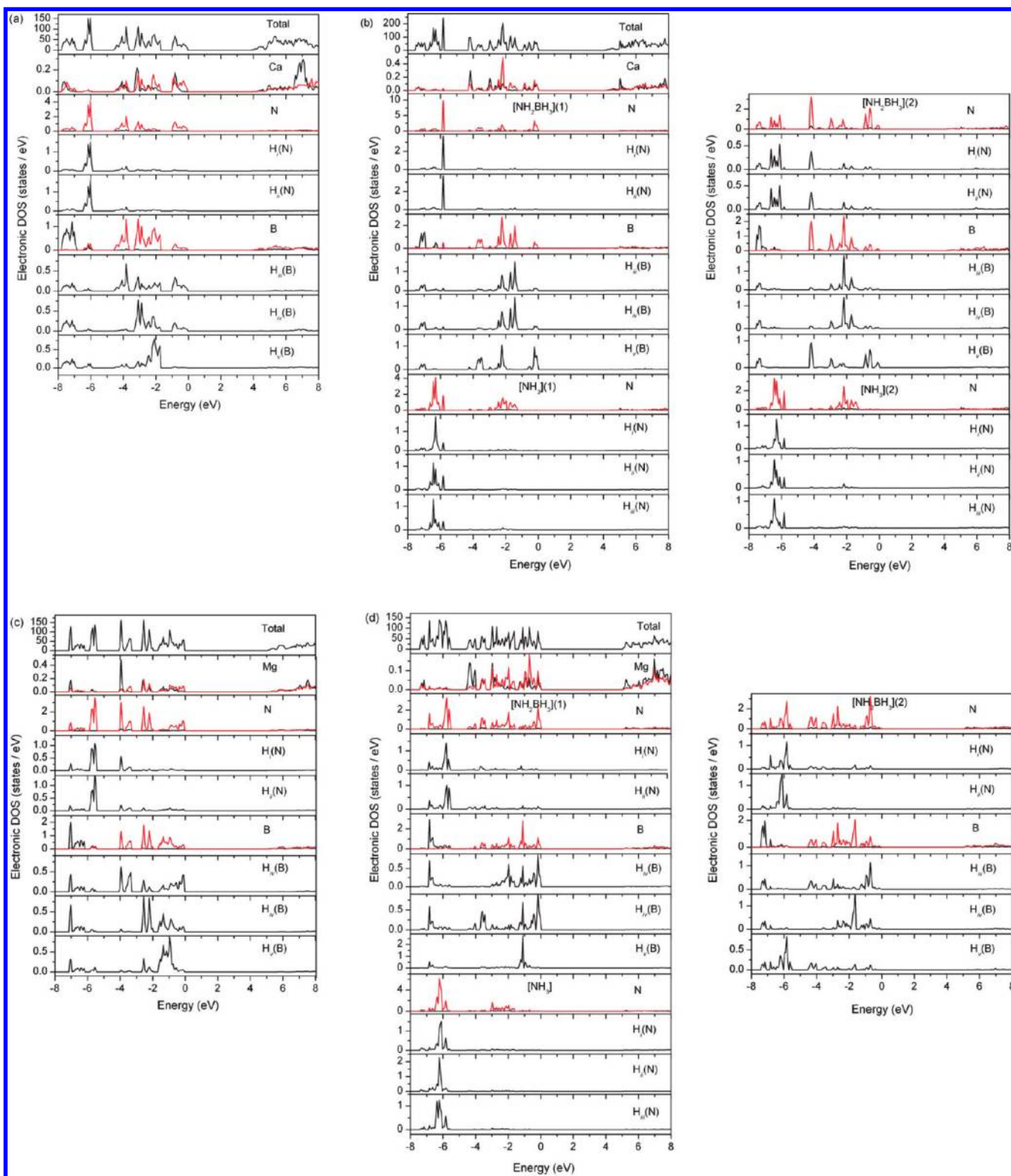


**Figure 2.** Total and partial electronic DOS of (a)  $\text{Ca}(\text{NH}_2\text{BH}_3)_2$ , (b)  $\text{Ca}(\text{NH}_2\text{BH}_3)_2 \cdot 2\text{NH}_3$ , (c)  $\text{Mg}(\text{NH}_2\text{BH}_3)_2$ , and (d)  $\text{Mg}(\text{NH}_2\text{BH}_3)_2 \cdot \text{NH}_3$ . s-Electron contributions are depicted with black solid line, and p-states are depicted with red solid line. The numbers (1) and (2) in the parentheses denote symmetrically nonequivalent  $[\text{NH}_2\text{BH}_3]$  complexes or  $[\text{NH}_3]$  molecules.

of CaAB is comparable with that in the  $[\text{AB}](1)_{\text{II}}$  (1.540 Å) and  $[\text{AB}](2)_{\text{II}}$  (1.553 Å) of  $\text{CaAB} \cdot 2\text{NH}_3$ . The B–H and N–H bonds have various lengths in symmetrically nonequivalent  $[\text{AB}]$  anions and  $[\text{NH}_3]$  molecules. The mean B–H and N–H bond lengths in  $[\text{AB}]$  anions of CaAB and  $\text{CaAB} \cdot 2\text{NH}_3$  can be taken as equal. The N–H bonds (1.026 Å) in  $[\text{NH}_3]_{\text{II}}$  molecule

are slightly longer than the N–H bonds (1.020 and 1.022 Å) in  $[\text{AB}]_{\text{II}}$  anion. The H(B) atoms in MgAB and  $\text{MgAB} \cdot \text{NH}_3$  facing Mg cation have much shorter distances from Mg ( $\sim 2.0$  Å) than the  $\text{Ca} \cdots \text{H}(\text{B})$  distance ( $\sim 2.4$  Å) in CaAB and  $\text{CaAB} \cdot 2\text{NH}_3$ , indicating a stronger electrostatic coordination between Mg cation and H(B). The shortest  $\text{Mg}_{\text{III}} \cdots \text{H}(\text{B})_{\text{III}}$  distance of 2.001

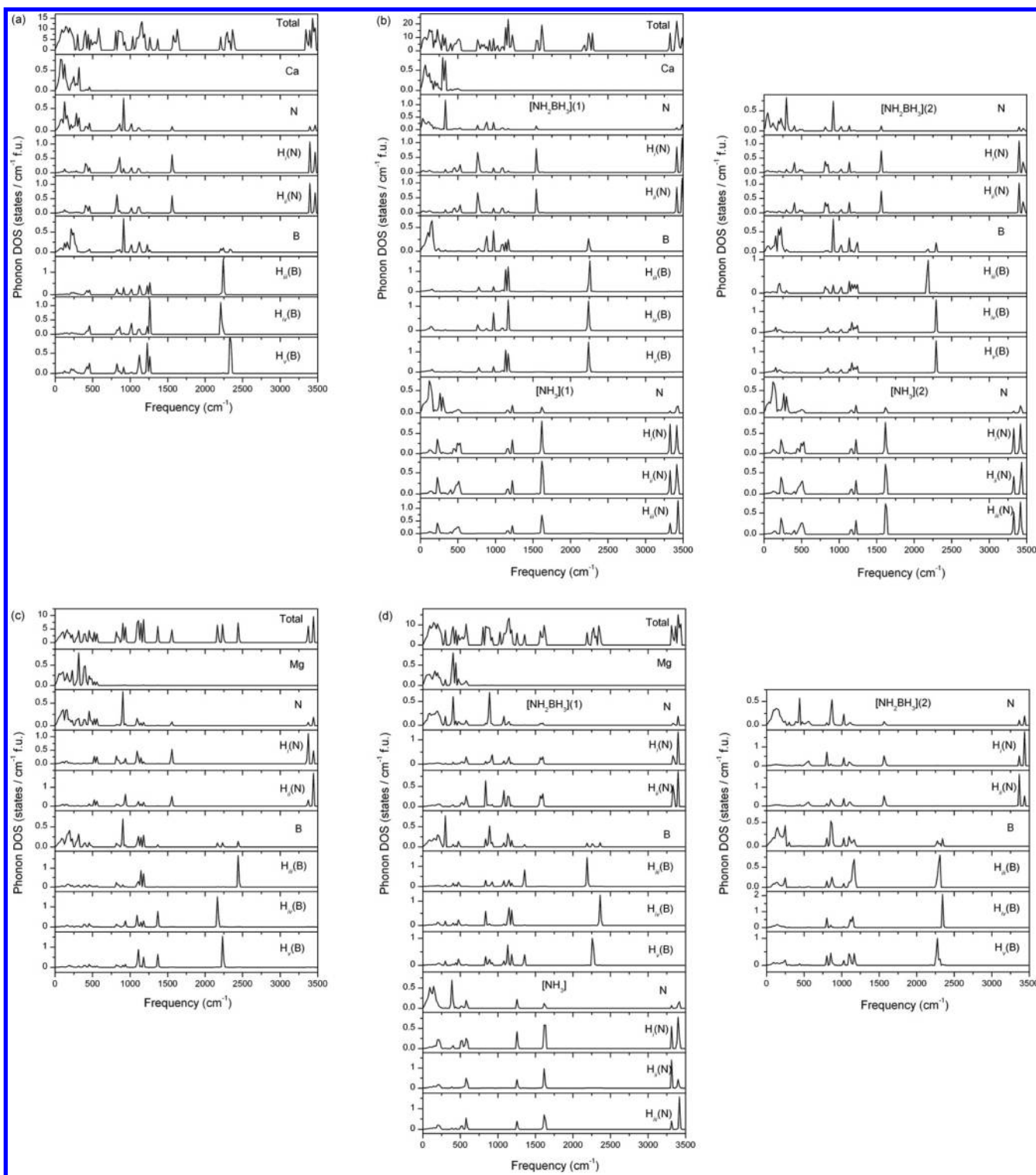


**Figure 3.** Total and partial phonon DOS of (a)  $\text{Ca}(\text{NH}_2\text{BH}_3)_2$ , (b)  $\text{Ca}(\text{NH}_2\text{BH}_3)_2 \cdot 2\text{NH}_3$ , (c)  $\text{Mg}(\text{NH}_2\text{BH}_3)_2$ , and (d)  $\text{Mg}(\text{NH}_2\text{BH}_3)_2 \cdot \text{NH}_3$ . The numbers (1) and (2) in the parentheses denote symmetrically nonequivalent  $[\text{NH}_2\text{BH}_3]$  complexes or  $[\text{NH}_3]$  molecules.

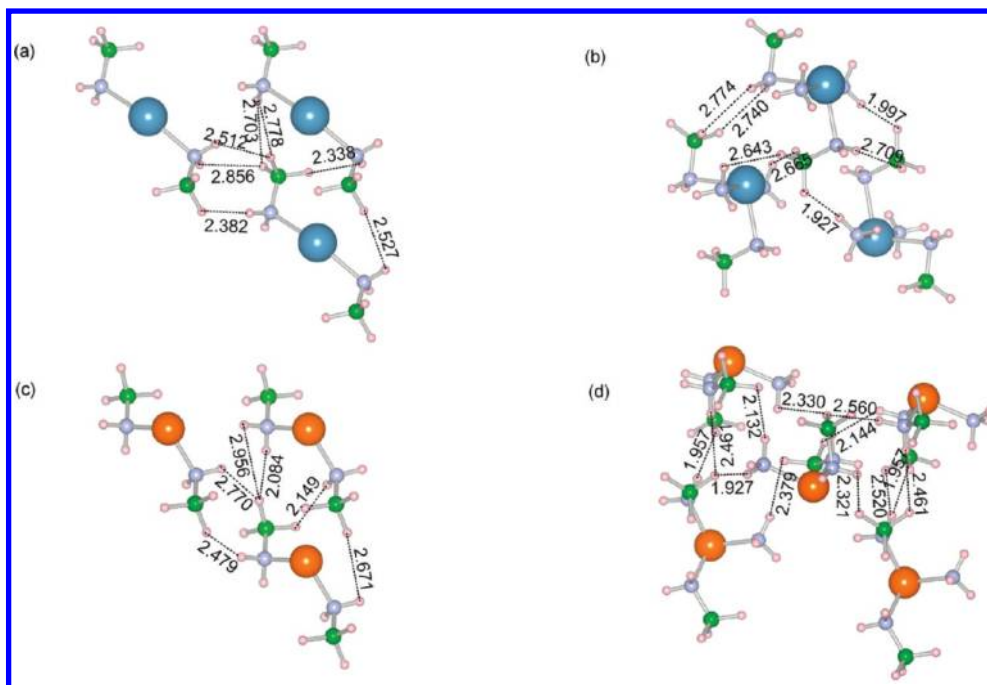
Å in MgAB is comparable with that in  $\text{MgAB} \cdot \text{NH}_3$  (1.993 Å). The B–N bond lengths are around 1.56 Å in MgAB and  $\text{MgAB} \cdot \text{NH}_3$ , slightly longer than that in CaAB and  $\text{CaAB} \cdot 2\text{NH}_3$  (~1.54 Å). The mean B–H and N–H bond lengths in [AB] anions of MgAB and  $\text{MgAB} \cdot \text{NH}_3$  are more or less the same. The N–H bonds in  $[\text{NH}_3]$  molecule of  $\text{MgAB} \cdot \text{NH}_3$  are slightly longer than those in [AB] anions, similar to the situation in  $\text{CaAB} \cdot 2\text{NH}_3$ .

The distance of  $\text{H}(\text{B}) \cdots \text{H}(\text{N})$  is one of the characteristic parameters for the crystal stability of the metal–B–N–H containing chemical hydride system.<sup>8</sup> Figure 4 demonstrates the intermolecular  $\text{H}(\text{B}) \cdots \text{H}(\text{N})$  coordination network in the derived molecules in all systems. Among triple neighboring molecules in CaAB and MgAB, the  $\text{H}(\text{B}) \cdots \text{H}(\text{N})$  distances are in the range of 2.338–2.856 Å and 2.084–2.956 Å, respectively. While in  $\text{CaAB} \cdot 2\text{NH}_3$  and  $\text{MgAB} \cdot \text{NH}_3$ , the  $\text{H}(\text{B}) \cdots \text{H}(\text{N})$

**Table 2.** Calculated Interatomic Distances (Å) in  $\text{Ca}(\text{NH}_2\text{BH}_3)_2$  (CaAB),  $\text{Ca}(\text{NH}_2\text{BH}_3)_2 \cdot 2\text{NH}_3$  (CaAB·2NH<sub>3</sub>),  $\text{Mg}(\text{NH}_2\text{BH}_3)_2$  (MgAB), and  $\text{Mg}(\text{NH}_2\text{BH}_3)_2 \cdot \text{NH}_3$  (MgAB·NH<sub>3</sub>)

Bonds	CaAB (I)	CaAB·2NH <sub>3</sub> (II)		MgAB (III)	MgAB·NH <sub>3</sub> (IV)	
	[AB] <sub>I</sub>	[AB](1) <sub>II</sub> <sup>a</sup>	[AB](2) <sub>II</sub>	[AB] <sub>III</sub>	[AB](1) <sub>IV</sub>	[AB](2) <sub>IV</sub>
Ca/Mg–N <sub>[AB]</sub>	2.476	2.397	2.470	2.111	2.104	2.104
Ca/Mg···H(B)	2.363		2.421	2.001	1.993	2.126
B–N <sub>[AB]</sub>	1.546	1.540	1.553	1.556	1.558	1.569
B–H <sub>i</sub>	1.229	1.240	1.236	1.213	1.223	1.226
B–H <sub>ii</sub>	1.242	1.242	1.236	1.245	1.240	1.234
B–H <sub>iii</sub>	1.249	1.242	1.251	1.254	1.251	1.241
B–H <sub>mean</sub>	1.240	1.241	1.241	1.237	1.238	1.234
N <sub>[AB]</sub> –H <sub>iv</sub>	1.022	1.020	1.022	1.023	1.026	1.023
N <sub>[AB]</sub> –H <sub>v</sub>	1.022	1.020	1.022	1.025	1.026	1.025
N <sub>[AB]</sub> –H <sub>mean</sub>	1.022	1.020	1.022	1.024	1.026	1.024
		[NH <sub>3</sub> ](1) <sub>II</sub>	[NH <sub>3</sub> ](2) <sub>II</sub>		[NH <sub>3</sub> ] <sub>IV</sub>	
Ca/Mg–N <sub>[NH<sub>3</sub>]</sub>		2.517	2.521		2.157	
N <sub>[NH<sub>3</sub>]</sub> –H <sub>vi</sub>		1.026	1.026		1.025	
N <sub>[NH<sub>3</sub>]</sub> –H <sub>vii</sub>		1.026	1.026		1.027	
N <sub>[NH<sub>3</sub>]</sub> –H <sub>viii</sub>		1.027	1.026		1.028	
N <sub>[NH<sub>3</sub>]</sub> –H <sub>mean</sub>		1.026	1.026		1.027	
H(B)···H(N)	2.338–2.856	1.927–2.774		2.084–2.956	1.927–2.560	

<sup>a</sup>The numbers (1) and (2) in the parentheses denote symmetrically nonequivalent [AB] anions or [NH<sub>3</sub>] molecules coordinated with Ca/Mg cation.

**Figure 4.** Intermolecular H(B)···H(N) coordination network in the derived molecules of (a)  $\text{Ca}(\text{NH}_2\text{BH}_3)_2$ , (b)  $\text{Ca}(\text{NH}_2\text{BH}_3)_2 \cdot 2\text{NH}_3$ , (c)  $\text{Mg}(\text{NH}_2\text{BH}_3)_2$ , and (d)  $\text{Mg}(\text{NH}_2\text{BH}_3)_2 \cdot \text{NH}_3$ . Distances of H(B)···H(N) are indicated, with units in Angstrom. The large blue, large orange, small light blue, small green, small pink spheres denote Ca, Mg, N, B, and H atom, respectively.

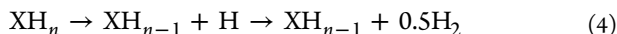
distances among neighboring molecules are much shorter than those in CaAB and MgAB due to the presence of [NH<sub>3</sub>] molecules. For example, the shortest H(B)···H(N) distance between a [BH<sub>3</sub>] group and a nearby [NH<sub>3</sub>] molecule in CaAB·2NH<sub>3</sub> and MgAB·NH<sub>3</sub> is ~1.927 Å, indicating a strong dihydrogen bonding interaction. Moreover, in Figure 4d we can see that the dihydrogen bonding network in MgAB·NH<sub>3</sub> is more intensive than that in other systems, showing a stronger interaction between [AB] anions and nearby [NH<sub>3</sub>] molecules.

Because of these strong dihydrogen interactions, the detachments of hydridic H(B) and protic H(N) atoms and subsequent combination could occur at lower temperature in the ammoniates compared to those in the corresponding metal amidoboranes, which we will elaborate below.

**3.5. Hydrogen Removal Energy and the First-Step Dehydrogenation.** In addition to the qualitative analyses on bond lengths, we further worked on quantitative investigations on the B–H and N–H bonds strength by calculating hydrogen



removal energy since the strength of hydrogen-host bonds can be quantified by the change in cohesive energy before and after the dissociation of hydrogen atom from the system.<sup>27</sup> The hydrogen atom removal process is specified as



in which  $\text{XH}_n$  and  $\text{XH}_{n-1}$  denote the solid system containing  $n$  hydrogen atoms and the system with one hydrogen atom removed, respectively, and the removed hydrogen atom is desorbed to vacuum to associatively form a  $\text{H}_2$  molecule. The hydrogen atom removal energy is defined accordingly as,

$$\Delta E_{\text{H}} = E_{\text{coh}}[\text{XH}_{n-1}] + 0.5E_{\text{coh}}[\text{H}_2] - E_{\text{coh}}[\text{XH}_n] \quad (5)$$

where  $E_{\text{coh}}$  is cohesive energy, the difference between the electronic total energy of the atoms of a solid and the sum of the total energy of individual free atoms. The hydrogen atom within the longest B–H or N–H bond was chosen to be removed in each solid structure. Atomic coordination of the targeted structure with hydrogen vacancy was fully reoptimized.

The calculated hydrogen atom removal energies are summarized in Table 3. Generally, H(B) removal energies are

**Table 3. H(B) and H(N) Atom Removal Energies<sup>a</sup> ( $\Delta E_{\text{H}}$ , eV) in  $\text{Ca}(\text{NH}_2\text{BH}_3)_2$  (CaAB),  $\text{Ca}(\text{NH}_2\text{BH}_3)_2 \cdot 2\text{NH}_3$  (CaAB·2NH<sub>3</sub>),  $\text{Mg}(\text{NH}_2\text{BH}_3)_2$  (MgAB), and  $\text{Mg}(\text{NH}_2\text{BH}_3)_2 \cdot \text{NH}_3$  (MgAB·NH<sub>3</sub>)**

	CaAB	CaAB·2NH <sub>3</sub>	MgAB	MgAB·NH <sub>3</sub>
$\Delta E_{\text{H(B)}}$	2.016	1.919	1.684	2.031
$\Delta E_{\text{H(N)}}$	2.490	2.731	2.471	3.085

<sup>a</sup>The hydrogen atom removal energy is defined as  $\Delta E_{\text{H}} = E_{\text{coh}}[\text{XH}_{n-1}] + 0.5E_{\text{coh}}[\text{H}_2] - E_{\text{coh}}[\text{XH}_n]$ , in which  $E_{\text{coh}}$  is the cohesive energy, the difference between the electronic total energy of the atoms of a solid and the sum of the total energy of individual free atoms.  $\text{XH}_n$  and  $\text{XH}_{n-1}$  denote the solid system containing  $n$  hydrogen atoms and the system with one hydrogen atom being removed, respectively.

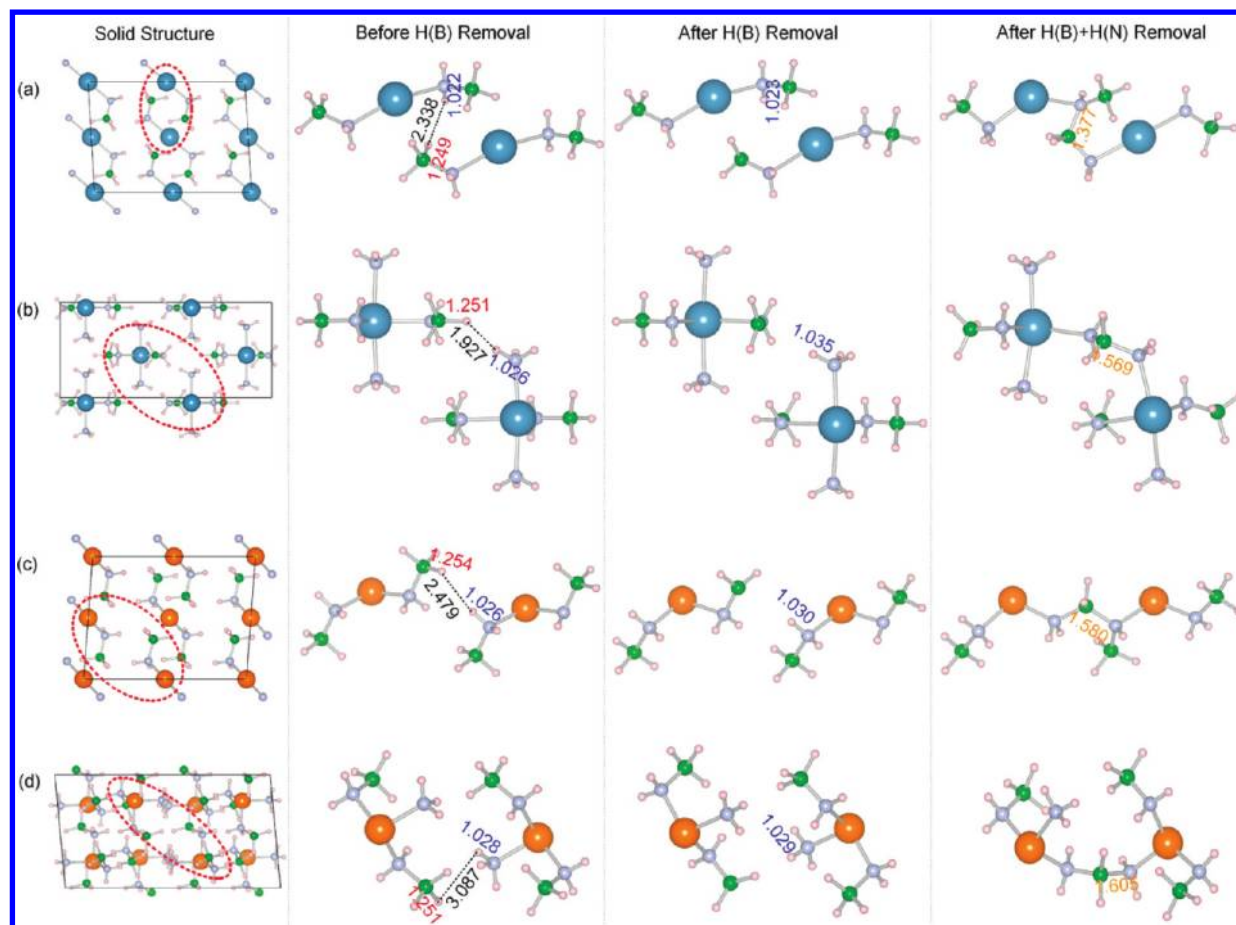
lower than H(N) removal energies, indicating that hydrogen atoms are more weakly attached with B atom than that with N; therefore, it is reasonable to deduce that the H(B) atom is detached from the system prior to the H(N) atom in the initial process of the dehydrogenation. We notice that the calculated H(B) atom removal energy of MgAB is relatively lower than in other materials, which could reflect the instability of MgAB, and it is indeed experimentally observed to be unstable at room temperature. Unlike CaAB or SrAB, the condensed charge borne by a small  $\text{Mg}^{2+}$  cation (0.65 Å) cannot be effectively compensated by the relatively large two  $[\text{NH}_2\text{BH}_3]^-$  anions, leading to an unstable structure under ambient condition.<sup>16</sup> A recent density functional calculation based on metal amidoboranes MAB (M = Li, Na, K, Ca, Be, Al) molecules showed that the molecular MgAB possesses the less negative cohesive energy compared to other MAB, implying its structural instability, and it is easier to be decomposed than any other metal amidoboranes under the same temperature condition.<sup>38</sup> From the above evidence, we may understand why the crystal solid-phase of MgAB has not been detected so far in experiments.

Figure 5 displays dimolecule motif derived from the optimized crystal solid structure of each system before and after removing H(B) atom (in the longest B–H bond). In the

reoptimized structure of CaAB after removing  $\text{H}_1(\text{B})$  atom, it is interesting to discover that the  $\text{N}_1\text{--H}_1$  bond nearby the removed  $\text{H}(\text{B})_1$  site becomes the longest N–H length in the local structure (see the third column of Figure 5a). Because of its relatively longer bond length, the dissociation of this  $\text{N}_1\text{--H}_1$  bond is consequently preferential over other N–H bonds. Reverting to examine the structure before removing  $\text{H}(\text{B})_1$  atom, we find that the distance of  $\text{H}(\text{B})_1 \cdots \text{H}(\text{N})_1$  coordination is 2.338 Å (see the second column of Figure 5a). This distance leads to an intermolecular dihydrogen coordination between two neighboring [AB] anions, i.e.,  $[\text{H}_2\text{NH}_2\text{B-}] \cdots \text{H}[-\text{NH}_2\text{BH}_3]$ , which is exactly the shortest dihydrogen bond length in CaAB. The associated hydridic  $\text{B}_1\text{--H}_1$  and protic  $\text{N}_1\text{--H}_1$  bonds lengths of 1.249 Å and 1.022 Å happen to be the longest B–H and N–H bonds in the local solid structure of CaAB. Therefore, we propose that because of the dihydrogen interaction, the dissociation of first hydridic  $\text{B}_1\text{--H}_1$  bond promotes the breaking of its adjacent protic  $\text{N}_1\text{--H}_1$  bond and the consequent detachment of the  $\text{H}(\text{N})_1$  atom. It is intriguing to know the effect of removing the dihydrogen coordinated  $\text{H}(\text{B})_1$  and  $\text{H}(\text{N})_1$  at the same time, that is, removing a  $\text{H}_2$  molecule. After removing  $\text{H}(\text{B})_1$  and  $\text{H}(\text{N})_1$  atoms from the lattice of CaAB and reoptimizing the structure, the  $\text{B}_1$  atom (in the hydridic  $\text{B}_1\text{--H}_1$  bond) and the  $\text{N}_1$  atom (in the protic  $\text{N}_1\text{--H}_1$  bond) coordinate with each other to form a new  $\text{B}_1\text{--N}_1$  bond with a bond distance of 1.550 Å (see the fourth column of Figure 5a). Although the above calculations hardly depict the real reaction path, those results provided a hint that the first-step dehydrogenation of CaAB may be through an intermolecular interaction with the dissociation and combination of H(B) and H(N) from two neighboring [CaAB] molecules.

It is worth noting that the  $\text{H}(\text{B})_{\text{II}}$  atom (in the longest B–H bond) in CaAB·2NH<sub>3</sub> locates in a  $[\text{AB}]_{\text{II}}$  anion; after removing  $\text{H}(\text{B})_{\text{II}}$ , the longest  $\text{N}_{\text{II}}\text{--H}_{\text{II}}$  bond (with a length of 1.035 Å) was found to locate in an adjacent  $[\text{NH}_3]_{\text{II}}$  molecule (see the third column of Figure 5b). In fact,  $\text{H}(\text{B})_{\text{II}}$  (before its removal) forms the shortest dihydrogen bond (with a length of 1.927 Å) with that  $\text{H}(\text{N})_{\text{II}}$  atom in the pristine structure (see the second column of Figure 5b). Hence, the presence of the  $[\text{NH}_3]$  molecules in the structure induces stronger intermolecular interaction of  $\text{H}(\text{B}) \cdots \text{H}(\text{N})$  between [AB] anions and  $[\text{NH}_3]$  molecules to facilitate the breaking of the B–H and N–H bonds, which is likely to be the main path for the first-step dehydrogenation of CaAB·2NH<sub>3</sub>. After  $\text{H}_2$  removal, the associated B and N connected with each other to form a new  $\text{B}_{\text{II}}\text{--N}_{\text{II}}$  bond with a length of 1.569 Å (see the fourth column of Figure 5b).

Similar to CaAB, after removing the  $\text{H}(\text{B})_{\text{III}}$  (in the longest B–H bond), the longest  $\text{N}_{\text{III}}\text{--H}_{\text{III}}$  bond (1.030 Å) appears nearby the removed  $\text{H}(\text{B})_{\text{III}}$  atom in the reoptimized MgAB structure (see the third column of Figure 5c). Looking back to the pristine structure, the distance of  $\text{H}(\text{B})_{\text{III}} \cdots \text{H}(\text{N})_{\text{III}}$  (2.479 Å) is a slightly longer than twice the van der Waals radius of hydrogen atom, and the associated hydridic  $\text{B}_{\text{III}}\text{--H}_{\text{III}}$  and protic  $\text{N}_{\text{III}}\text{--H}_{\text{III}}$  bonds (with lengths of 1.254 Å and 1.026 Å, respectively) are also the longest B–H and N–H bonds in the local structure of MgAB (see the second column of Figure 5c). After removing both  $\text{H}(\text{B})_{\text{III}}$  and  $\text{H}(\text{N})_{\text{III}}$  atoms, the  $\text{B}_{\text{III}}$  atom and  $\text{N}_{\text{III}}$  atom coordinate with each other to form a  $\text{B}_{\text{III}}\text{--N}_{\text{III}}$  bond with a distance of 1.580 Å (see the fourth column of Figure 5c).



**Figure 5.** Derived dimolecular motif from the optimized structure of (a)  $\text{Ca}(\text{NH}_2\text{BH}_3)_2$ , (b)  $\text{Ca}(\text{NH}_2\text{BH}_3)_2 \cdot 2\text{NH}_3$ , (c)  $\text{Mg}(\text{NH}_2\text{BH}_3)_2$ , and (d)  $\text{Mg}(\text{NH}_2\text{BH}_3)_2 \cdot \text{NH}_3$  before removing H(B) atom (2nd column), after removing H(B) atom (3rd column), and after removing H(B)+H(N), i.e.,  $\text{H}_2$  molecule (4th column). The H(B)···H(N) distance between H(B) (chosen to be removed) and the nearby H(N) atom, the associated B–H and N–H bond lengths, and the established B–N bond lengths are denoted in black, red, blue, and orange, respectively, in angstrom units. The large blue, large orange, small light blue, small green, small pink spheres denote Ca, Mg, N, B, and H atom, respectively.

In the optimized structure after removing a  $\text{H}(\text{B})_{\text{IV}}$  atom (in the longest B–H bond) in  $\text{MgAB} \cdot \text{NH}_3$ ; the longest  $\text{N}_{\text{IV}}\text{--H}_{\text{IV}}$  bond (1.029 Å) is, similarly, located within the nearby  $[\text{NH}_3]$  molecule (see the third column of Figure 5d). By further removing the  $\text{H}(\text{N})_{\text{IV}}$  atom, a new  $\text{B}_{\text{IV}}\text{--N}_{\text{IV}}$  bond is established with the length of 1.650 Å (see the fourth column of Figure 5d). So the first-step dehydrogenation of  $\text{MgAB} \cdot \text{NH}_3$  could be also described as the dissociation of a  $\text{H}(\text{B})_{\text{IV}}$  atom from  $[\text{AB}]$  anion and a  $\text{H}(\text{N})_{\text{IV}}$  atom from the nearby  $[\text{NH}_3]$  molecule and the subsequent coordination of the B and N atoms.

The previous experimental and theoretical studies on  $\text{NH}_3\text{BH}_3$ <sup>39,40</sup> and  $\text{LiNH}_2\text{BH}_3$ <sup>18,41,42</sup> indicated that the break-up of B–H bonds is involved in the rate-limiting step and affects the initial state of dehydrogenation of metal–B–N–H chemical hydride system. Thus, the H(B) removal energy may partially reflect the kinetic aspect of the dehydrogenation. However, it should be noted that the energy cost for removing a hydrogen atom to the vacuum from the material would have certain difference from the energy needed to transfer a hydride within the material to allow it to combine with a proton nearby to form a  $\text{H}_2$  molecule. Nutt et al.<sup>19</sup> and Kim et al.<sup>18</sup> speculated a “metal assisted hydride transfer” path via transferring hydridic H from  $[\text{BH}_3]$  to Li cation, and getting close to protic H in  $[\text{NH}_2]$  in the first-step dehydrogenation of  $\text{LiAB}$  based on the gas-phase molecular simulation. We believe that the metal

cation plays an essential role for the dissociation of H(B); however, it is difficult to identify such a transition state in our solid-state calculations, and  $\text{MgH}_2$  or  $\text{CaH}_2$  was not detected in our experiments.

**3.6. Hydrogen Diffusion in Solid CaAB,  $\text{CaAB} \cdot 2\text{NH}_3$ , and  $\text{MgAB} \cdot \text{NH}_3$ .** Diffusion of hydrogen through the lattice to the surface is an inherent step in the dehydrogenation of metal hydrides.<sup>43,44</sup> It is of interest to investigate the possible diffusion paths of hydrogen in chemical hydrides of CaAB,  $\text{CaAB} \cdot 2\text{NH}_3$ , and  $\text{MgAB} \cdot \text{NH}_3$  to figure out whether there would be some unique features. Hydrogen atoms could diffuse along various directions via several possible pathways to go through the lattice. Practically the most favorable path is determined by searching the lowest hydrogen migration energy. We first created a hydrogen vacancy in each solid structure by removing a H(B) atom, and a compensating background charge must be included to prevent divergence of the total energy. A series of possible pathways were designed to fill this  $[\text{V}_{\text{H}(\text{B})}]^+$  vacancy with the neighboring H(B) atom, and the migration energy was subsequently calculated for each pathway.

By searching several possible pathways via different directions to access to the vacancy  $[\text{V}_{\text{H}(\text{B})}]^+$  in CaAB, we found that the most likely diffusion pathway of a H(B) atom through the whole lattice of CaAB consists of a series of equivalent jumps along the  $[010]$  direction (see Figure 6a). A



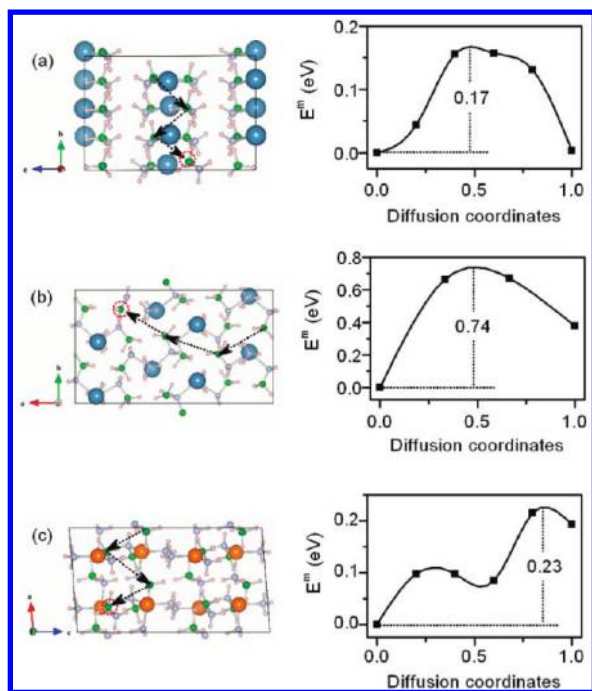


**Figure 6.** Schematic direction of the diffusion pathway of hydrogen atom and the diffusion energy profile of the diffusion unit-step in (a)  $\text{Ca}(\text{NH}_2\text{BH}_3)_2$ , (b)  $\text{Ca}(\text{NH}_2\text{BH}_3)_2 \cdot 2\text{NH}_3$ , and (c)  $\text{Mg}(\text{NH}_2\text{BH}_3)_2 \cdot \text{NH}_3$ . The energy barrier for each unit step is estimated by the energy difference between saddle point and initial state. The large blue, large orange, small light blue, small green, small pink spheres denote Ca, Mg, N, B, and H atoms, respectively.

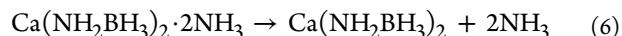
unit-jump (denoted by an arrowhead mark in Figure 6) is defined as to fill a charged vacancy  $[\text{V}_{\text{H(B)}}]^+$  in one  $[\text{BH}_3]$  group with a H(B) atom in the nearest  $[\text{BH}_3]$  group from the adjacent  $[\text{CaAB}]$  molecule. The diffusion energy barrier of the unit-jump, the energy difference between the saddle point and the initial state in the energy profile, is estimated to be 0.17 eV. Because of the symmetrical equivalence of  $[\text{AB}]$  anions in CaAB, each unit-jump from one  $[\text{BH}_3]$  group to the adjacent  $[\text{BH}_3]$  group is equivalent and should have the same energy barrier. Therefore the overall energy barrier of a H(B) atom diffusing through the solid lattice of CaAB along the  $[010]$  direction is regarded as 0.17 eV. The most likely diffusion pathway of a H(B) atom through the whole lattice of  $\text{CaAB} \cdot 2\text{NH}_3$  consists of a series of equivalent jumps along the  $[100]$  direction (see Figure 6b). The diffusion energy barrier for each unit-jump, to fill the charged vacancy  $[\text{V}_{\text{H(B)}}]^+$  with a hydrogen atom H(B) from the nearest  $[\text{BH}_3]$  group in the adjacent  $[\text{CaAB} \cdot 2\text{NH}_3]$  molecule, is determined to be 0.74 eV. The diffusion pathway of a H(B) atom through the lattice of  $\text{MgAB} \cdot \text{NH}_3$  is most favorable along the  $[100]$  direction, consisting of a series of equivalent jumps with the energy barrier of 0.23 eV (see Figure 6c).

Compared to the diffusion barrier in CaAB (0.17 eV) and  $\text{MgAB} \cdot \text{NH}_3$  (0.23 eV), the H(B) atom needs to overcome a relatively higher energy barrier in  $\text{CaAB} \cdot 2\text{NH}_3$  (0.74 eV) to diffuse from its original position in the  $[\text{BH}_3]$  group to the nearby  $[\text{V}_{\text{H(B)}}]^+$  vacancy in the adjacent  $[\text{BH}_3]$  group. This could be explained by the geometrical transformation caused by the involvement of the  $[\text{NH}_3]$  molecule. As two  $[\text{NH}_3]$  molecules coordinated with one Ca cation in  $\text{CaAB} \cdot 2\text{NH}_3$ , the positions of  $[\text{AB}]$  anions become dispersed that B...B distance (4.75 Å) between two adjacent  $[\text{BH}_3]$  groups is much longer

than that of 3.86 Å in CaAB. Therefore, the  $[\text{NH}_3]$  molecules in  $\text{CaAB} \cdot 2\text{NH}_3$  act as a “disperser”, leading to a wider distribution of groups and molecules, and subsequently raising the energy barrier for hydrogen diffusion in a longer range distance. While in  $\text{MgAB} \cdot \text{NH}_3$ , the coordination of a single  $[\text{NH}_3]$  molecule on each Mg cation affects the positions of  $[\text{AB}]$  anions, but has less impact on the density of distribution of  $[\text{AB}]$  anions, as the B...B distance of 3.78 Å between two adjacent  $[\text{BH}_3]$  groups is comparable with that of 3.77 Å in MgAB.

The experiments have shown that the initiation of dehydrogenation of CaAB,  $\text{CaAB} \cdot 2\text{NH}_3$ , and  $\text{MgAB} \cdot \text{NH}_3$  happened at  $\sim 353$  K,  $\sim 343$  K, and  $\sim 323$  K, respectively. This could reflect the magnitude of activation energies in the order of  $\text{MgAB} \cdot \text{NH}_3 < \text{CaAB} \cdot 2\text{NH}_3 < \text{CaAB}$  for hydrogen release. Combined H(B) migration energies with the preceding calculated H(B) hydrogen removal energies results, particularly in  $\text{CaAB} \cdot 2\text{NH}_3$ , although with a lower H(B) removal energy of 1.92 eV, the H(B) diffusion energy barrier of 0.74 eV is relatively higher among the three systems. Thus, we speculate that the activation energy to be overcome in the initiation of dehydrogenation could be related not only with the break-up of B–H bond but also with the diffusion of H(B) through the lattice. To verify this speculation, a calculation of the activation energy is required in future work.

**3.7. Deammoniation Thermodynamics of  $\text{CaAB} \cdot 2\text{NH}_3$  and  $\text{MgAB} \cdot \text{NH}_3$ .** The decomposition of  $\text{CaAB} \cdot 2\text{NH}_3$  under dynamic flow mode is described in the following reaction<sup>13</sup>



The released gaseous product is mainly ammonia at temperatures below 373 K, and set-off deammoniation temperature is  $\sim 323$  K, while the decomposition of  $\text{MgAB} \cdot \text{NH}_3$  is remarkably different from that of  $\text{CaAB} \cdot 2\text{NH}_3$  in that the release of  $\text{H}_2$  with minor  $\text{NH}_3$  was detected to start from  $\sim 323$  K. To figure out such a difference we calculated deammoniation enthalpies of  $\text{CaAB} \cdot 2\text{NH}_3$  and  $\text{MgAB} \cdot \text{NH}_3$ , respectively. The deammoniation enthalpy of  $\text{CaAB} \cdot 2\text{NH}_3$ , the difference of the formation enthalpies between reactant and products, can be estimated as follows:

$$\begin{aligned} \Delta H_{\text{R}} &= \Delta H_{\text{Ca}(\text{NH}_2\text{BH}_3)_2} + 2\Delta H_{\text{NH}_3} \\ &\quad - \Delta H_{\text{Ca}(\text{NH}_2\text{BH}_3)_2 \cdot 2\text{NH}_3} \end{aligned} \quad (7)$$

where  $\Delta H$  is the formation enthalpy of materials involved in the reaction, which can be calculated with respect to the enthalpy of the neutral phase of each element,

$$\begin{aligned} \Delta H_{\text{Ca}(\text{NH}_2\text{BH}_3)_2} &= H_{\text{Ca}(\text{NH}_2\text{BH}_3)_2} - H_{\text{Ca}} - H_{\text{N}_2} - 2H_{\text{B}} - 5H_{\text{H}_2} \end{aligned} \quad (8)$$

$$\Delta H_{\text{NH}_3} = H_{\text{NH}_3} - 1/2H_{\text{N}_2} - 3/2H_{\text{H}_2} \quad (9)$$

$$\begin{aligned} \Delta H_{\text{Ca}(\text{NH}_2\text{BH}_3)_2 \cdot 2\text{NH}_3} &= H_{\text{Ca}(\text{NH}_2\text{BH}_3)_2 \cdot 2\text{NH}_3} - H_{\text{Ca}} - 2H_{\text{N}_2} - 2H_{\text{B}} \\ &\quad - 8H_{\text{H}_2} \end{aligned} \quad (10)$$

**Table 4.** Calculated Total Electronic Energy ( $E_{\text{elec}}^0$ , eV) at  $T = 0$  K, Vibrational Enthalpy ( $H_{\text{vib}}$ , kJ/mol), Entropy ( $S_{\text{vib}}/S_{\text{gas}}^\circ$ , J/K/mol)<sup>a</sup> Vibrational Helmholtz Free Energy ( $F_{\text{vib}}$ , kJ/mol) at  $T = 300$  K of Reactant and Products Involved in the Deammoniation Reactions of  $\text{Ca}(\text{NH}_2\text{BH}_3)_2 \cdot 2\text{NH}_3$  and  $\text{Mg}(\text{NH}_2\text{BH}_3)_2 \cdot \text{NH}_3$

	$\text{Ca}(\text{NH}_2\text{BH}_3)_2 \cdot 2\text{NH}_3$ (s)	$\text{Ca}(\text{NH}_2\text{BH}_3)_2$ (s)	$2\text{NH}_3$ (g)	$\Delta(\text{P-R})^b$
$E_{\text{elec}}^0$	-113.02	-72.82	$-19.60 \times 2$	1.02
$H_{\text{vib}}$	534.93	331.24	$92.50 \times 2$	-18.69
$S_{\text{vib}}/S_{\text{gas}}^\circ$	291.93	163.58	$192.99^c \times 2$	257.63 <sup>d</sup>
$F_{\text{vib}}$	447.35	282.16	$76.83 \times 2$	-11.53
$E_{\text{mole}}$			$9.98^d \times 2$	
	$\text{Mg}(\text{NH}_2\text{BH}_3)_2 \cdot \text{NH}_3$ (s)	$\text{Mg}(\text{NH}_2\text{BH}_3)_2$ (s)	$\text{NH}_3$ (g)	$\Delta(\text{P-R})$
$E_{\text{elec}}^0$	-91.53	-71.27	$-19.60 [-19.6^e]$	0.66
$H_{\text{vib}}$	439.20	335.91	$92.50 [87.9^f]$	-10.80
$S_{\text{vib}}/S_{\text{gas}}^\circ$	206.71	154.85	192.99	141.14
$F_{\text{vib}}$	377.19	289.45	$76.83 [87.78^f]$	-10.91
$E_{\text{mole}}$			9.98	

<sup>a</sup> $S_{\text{vib}}/S_{\text{gas}}^\circ$ ,  $S_{\text{vib}}$  is the vibrational entropy for solid-phase,  $S_{\text{gas}}^\circ$  is the standard molar entropy of a given molecular species in the gas phase at  $p = 1$  bar.

<sup>c</sup> $\Delta(\text{P-R})$  refers to the difference between reactant and products for each thermodynamic parameter.  $\Delta E_{\text{R}}^0$ ,  $\Delta H_{\text{R}}$ , and  $\Delta F_{\text{R}}$  refer to the changes in total electronic energy at  $T = 0$  K, enthalpy and Helmholtz Free energy at  $T = 300$  K, respectively, of the deammoniation reactions. 1 eV = 96.48534 kJ/mol. <sup>e</sup>The standard entropy of ammonia  $S_{\text{NH}_3}^\circ = A \ln(t) + Bt + Ct^2/2 + Dt^3/3 - E/(2t^2) + G$ , in which  $A = 19.99563$ ,  $B = 49.77119$ ,  $C = -15.37599$ ,  $D = 1.921168$ ,  $E = -0.189174$ ,  $F = -53.30667$ ,  $G = 203.8591$ ,  $t = T/1000$ . <sup>d</sup> $E_{\text{mole}} = 4k_{\text{B}}T$  for  $\text{NH}_3$ , accounting for translational ( $3/2k_{\text{B}}T$ ), rotational ( $3/2k_{\text{B}}T$ ), and  $pV$  ( $k_{\text{B}}T$ ). <sup>f</sup>Reference 47. <sup>g</sup>Reference 27.

Taking eqs 8–10 into eq 7, we get the reaction enthalpy as,

$$\Delta H_{\text{R}} = H_{\text{Ca}(\text{NH}_2\text{BH}_3)_2} + 2H_{\text{NH}_3} - H_{\text{Ca}(\text{NH}_2\text{BH}_3)_2 \cdot 2\text{NH}_3} \quad (11)$$

where  $H$  is enthalpy, which is defined as  $H = U + pV$ ,  $U$  is internal energy,  $p$  the pressure, and  $V$  the volume. For solid phase, the effect of pressure on the energy of solids is small, and the  $pV$  term can be neglected;<sup>45</sup> thus

$$H_{\text{solid}} \approx U = E_{\text{elec}}^0 + H_{\text{vib}}(T) \quad (12)$$

For a molecule (ammonia) in the gas phase, an additional term should be added in eq 12, that is,

$$H_{\text{molecule}} = E_{\text{elec}}^0 + H_{\text{vib}}(T) + E_{\text{mole}}(T) \quad (13)$$

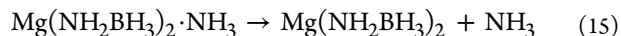
where  $E_{\text{mole}}(T)$  is the contribution from the translational ( $3/2k_{\text{B}}T$ ), rotational ( $3/2k_{\text{B}}T$  for  $\text{NH}_3$ ), as well as the  $pV$  terms ( $k_{\text{B}}T$ ) due to the molecular degrees of freedom. In eq 12 and 13,  $E_{\text{elec}}^0$  is total electronic energy at  $T = 0$  K calculated by first-principles calculations, and  $H_{\text{vib}}(T)$  is the vibrational enthalpy contribution at finite temperature  $T$ , which can be obtained within the harmonic approximation by

$$H_{\text{vib}}(T) = \frac{1}{2}r \int_0^\infty g(\omega) (\hbar\omega) \coth\left(\frac{\hbar\omega}{2k_{\text{B}}T}\right) d\omega \quad (14)$$

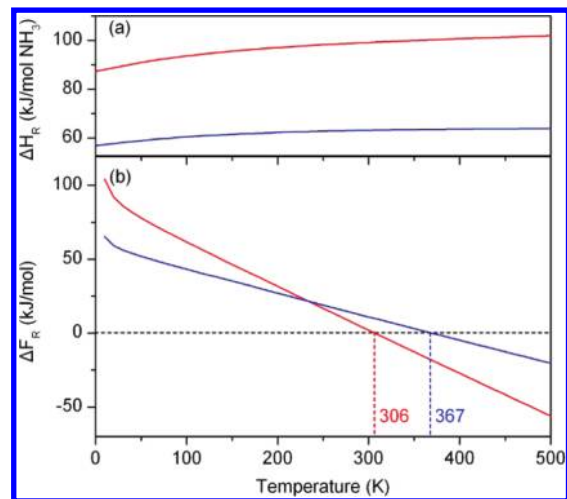
where  $T$  is temperature,  $r$  is the number of degrees of freedom,  $\hbar$  is reduced Planck constant,  $k_{\text{B}}$  is the Boltzmann constant, and  $g(\omega)$  and  $\omega$  are phonon DOS and frequencies obtained by the direct method.

Table 4 summarizes the thermodynamic parameters of reactant and products involved in the deammoniation reactions of  $\text{CaAB} \cdot 2\text{NH}_3$  and  $\text{MgAB} \cdot \text{NH}_3$ . These quantities, according to eq 11, yield the reaction enthalpy of deammoniation ( $\Delta H_{\text{R}}$ ) of  $\text{CaAB} \cdot 2\text{NH}_3$  as 99.20 kJ/mol at  $T = 300$  K. Vibrational effects are found to contribute trivially to the  $\text{CaAB} \cdot 2\text{NH}_3$  system as there is only a slight difference between  $\Delta H_{\text{R}}^{300\text{K}}$  (99.20 kJ/mol) and  $\Delta E_{\text{R}}^0$  (1.02 eV = 97.93 kJ/mol).

For comparison, we calculated the deammoniation enthalpy of  $\text{MgAB} \cdot \text{NH}_3$  by assuming it undergoes the reaction below,



By using the same method, we obtained the deammoniation enthalpy of  $\text{MgAB} \cdot \text{NH}_3$  as 63.24 kJ/mol at  $T = 300$  K. The deammoniation of both  $\text{CaAB} \cdot 2\text{NH}_3$  and  $\text{MgAB} \cdot \text{NH}_3$  are endothermic processes. Figure 7 displays the change in



**Figure 7.** Calculated change in (a) enthalpies ( $\Delta H_{\text{R}}$ ) and (b) Helmholtz free energy ( $\Delta F_{\text{R}}$ ) for the deammoniation reactions of  $\text{Ca}(\text{NH}_2\text{BH}_3)_2 \cdot 2\text{NH}_3$  (denoted as red line) and  $\text{Mg}(\text{NH}_2\text{BH}_3)_2 \cdot \text{NH}_3$  (denoted as blue line) as a function of temperature at  $p = 1$  bar.

enthalpies and free energies for the deammoniation reaction as a function of  $T$  in the temperature range of 0–500 K. It is noted that although with lower reaction enthalpy, the change in free energy for the deammoniation of  $\text{MgAB} \cdot \text{NH}_3$  turns to be negative above 367 K, indicating that deammoniation of  $\text{MgAB} \cdot \text{NH}_3$  could only occur beyond 367 K. While the change in free energy of  $\text{CaAB} \cdot 2\text{NH}_3$  becomes negative above 306 K, which is more thermodynamically favored than that of  $\text{MgAB} \cdot \text{NH}_3$ .

The different phenomena in the deammoniation of CaAB·2NH<sub>3</sub> and MgAB·NH<sub>3</sub> also reflect the different covalent interaction between [NH<sub>3</sub>] molecule and metal cation, and it is expected that the coordination between [NH<sub>3</sub>] and Mg cation is stronger than that between [NH<sub>3</sub>] and Ca cation. Therefore, we tested the coordination strength between Ca/Mg cation and [NH<sub>3</sub>] molecule by calculating the [NH<sub>3</sub>] molecule removal energy from the solid of CaAB·2NH<sub>3</sub> and MgAB·NH<sub>3</sub>, respectively. The [NH<sub>3</sub>] removal energies is calculated as

$$\Delta E_{\text{NH}_3} = E_{\text{coh}}[\text{XN}_{m-1}\text{H}_{n-3}] + E_{\text{coh}}[\text{NH}_3] - E_{\text{coh}}[\text{XN}_m\text{H}_n] \quad (16)$$

in which XN<sub>m</sub>H<sub>n</sub> and XN<sub>m-1</sub>H<sub>n-3</sub> denote the solid system containing *m* nitrogen atoms and *n* hydrogen atoms and the system with one [NH<sub>3</sub>] molecule being removed, respectively. We found that an additional energy of 0.56 eV is needed to dissociate one [NH<sub>3</sub>] molecule from MgAB·NH<sub>3</sub> than that from CaAB·2NH<sub>3</sub> (see Table 5), revealing a stronger

**Table 5.** [NH<sub>3</sub>] Removal Energy<sup>a</sup> (ΔE<sub>NH<sub>3</sub></sub>, eV) in the Supercell<sup>b</sup> of Ca(NH<sub>2</sub>BH<sub>3</sub>)<sub>2</sub>·2NH<sub>3</sub> and Mg(NH<sub>2</sub>BH<sub>3</sub>)<sub>2</sub>·NH<sub>3</sub>

[NH <sub>3</sub> ] removal	ΔE <sub>NH<sub>3</sub></sub>
Ca <sub>8</sub> N <sub>16</sub> H <sub>32</sub> B <sub>16</sub> H <sub>48</sub> ·N <sub>16</sub> H <sub>48</sub> → Ca <sub>8</sub> N <sub>16</sub> H <sub>32</sub> B <sub>16</sub> H <sub>48</sub> ·N <sub>15</sub> H <sub>45</sub> + NH <sub>3</sub>	0.42
Mg <sub>8</sub> N <sub>16</sub> H <sub>32</sub> B <sub>16</sub> H <sub>48</sub> ·N <sub>8</sub> H <sub>24</sub> → Mg <sub>8</sub> N <sub>16</sub> H <sub>32</sub> B <sub>16</sub> H <sub>48</sub> ·N <sub>7</sub> H <sub>21</sub> + NH <sub>3</sub>	0.98

<sup>a</sup>The [NH<sub>3</sub>] removal energy is defined as ΔE<sub>NH<sub>3</sub></sub> = E<sub>coh</sub>[XN<sub>m-1</sub>H<sub>n-3</sub>] + E<sub>coh</sub>[NH<sub>3</sub>] - E<sub>coh</sub>[XN<sub>m</sub>H<sub>n</sub>], in which E<sub>coh</sub> is the cohesive energy, the difference between the electronic total energy of the atoms of a solid and the sum of the total energy of individual free atoms. XN<sub>m</sub>H<sub>n</sub> and XN<sub>m-1</sub>H<sub>n-3</sub> denote the solid system containing *m* nitrogen atoms and *n* hydrogen atoms and the system with one [NH<sub>3</sub>] molecule being removed, respectively. <sup>b</sup>The 1 × 2 × 1 supercell of Ca(NH<sub>2</sub>BH<sub>3</sub>)<sub>2</sub>·2NH<sub>3</sub> contains 8 f.u., and the 1 × 1 × 2 supercell of Mg(NH<sub>2</sub>BH<sub>3</sub>)<sub>2</sub>·NH<sub>3</sub> contains 8 f.u.

interaction between the Mg cation and the [NH<sub>3</sub>] molecule. These results further explain why the deammoniation of MgAB·NH<sub>3</sub> hardly occurs.

#### 4. CONCLUSIONS

In this study, first-principles calculations were carried out on the solid calcium amidoborane ammoniate Ca(NH<sub>2</sub>BH<sub>3</sub>)<sub>2</sub>·2NH<sub>3</sub> (CaAB·2NH<sub>3</sub>) and magnesium amidoborane monoammoniate Mg(NH<sub>2</sub>BH<sub>3</sub>)<sub>2</sub>·NH<sub>3</sub> (MgAB·NH<sub>3</sub>) systems to study the role of the [NH<sub>3</sub>] molecule in improving the dehydrogenation properties of metal amidoborane monoammoniates compared to those of calcium amidoborane Ca(NH<sub>2</sub>BH<sub>3</sub>)<sub>2</sub> (CaAB) and magnesium amidoborane Mg(NH<sub>2</sub>BH<sub>3</sub>)<sub>2</sub> (MgAB). Our conclusions are summarized as follows:

- The analyses of crystal, electronic, and phononic structures indicate that the presence of [NH<sub>3</sub>] molecules prompts the formation of an intensive dihydrogen bonding network by supplying protic H and the activation of the B–H bonds in metal amidoborane monoammoniates, which could facilitate the desorption of H<sub>2</sub> from metal amidoborane ammoniates occurring at lower temperatures compared to the corresponding metal amidoboranes.
- The mechanism of first-step dehydrogenation is identified as the dissociation of the H(B) atom from the [NH<sub>2</sub>BH<sub>3</sub>]<sup>−</sup> anion and of the H(N) atom from

nearby [NH<sub>3</sub>] molecules, and the subsequent combination of H(B) and H(N) to form H<sub>2</sub>.

- The preliminary simulations of the hydrogen diffusion process through CaAB, CaAB·2NH<sub>3</sub>, and MgAB·NH<sub>3</sub> solid systems revealed that both the break-up of B–H bonds and the hydrogen diffusion are essential steps to affect the kinetics of the initiation of dehydrogenation of the metal–B–N–H chemical hydride systems.
- Finally, the deammoniation thermodynamics of CaAB·2NH<sub>3</sub> and MgAB·NH<sub>3</sub> based on phonon calculations showed that unlike CaAB·2NH<sub>3</sub>, the deammoniation of MgAB·NH<sub>3</sub> is only thermodynamically allowed at above 367 K. This incapability on deammoniation may help the [NH<sub>3</sub>] molecule to provide protic H for the dehydrogenation of MgAB·NH<sub>3</sub>. The calculations of [NH<sub>3</sub>] molecule removal energy show that the [NH<sub>3</sub>] molecule is more strongly coordinated with the Mg cation than with the Ca cation, which hinders NH<sub>3</sub> gas from detaching from MgAB·NH<sub>3</sub> at lower temperatures.

#### ■ ASSOCIATED CONTENT

##### Supporting Information

Structure parameters and atomic positions of Ca(NH<sub>2</sub>BH<sub>3</sub>)<sub>2</sub>, Ca(NH<sub>2</sub>BH<sub>3</sub>)<sub>2</sub>·2NH<sub>3</sub>, Mg(NH<sub>2</sub>BH<sub>3</sub>)<sub>2</sub>, and Mg(NH<sub>2</sub>BH<sub>3</sub>)<sub>2</sub>·NH<sub>3</sub>. This material is available free of charge via the Internet at <http://pubs.acs.org>.

#### ■ AUTHOR INFORMATION

##### Corresponding Author

\*E-mail: pchen@dicp.ac.cn. Phone: (+86) 411 84379583.

#### ■ ACKNOWLEDGMENTS

The authors acknowledge financial support from Hundred Talents Project and Knowledge Innovation Program of CAS (KGCX2-YW-806 and KJCX2-YW-H21), 973 Project (2010CB631304), the National Natural Science Foundation of China (No. 10979051 and 20973162), the National University of Singapore. The authors are also grateful to UPPMAX for providing computing time.

#### ■ REFERENCES

- Stephens, F. H.; Pons, V.; Tom Baker, R. *Dalton Trans.* **2007**, 2613.
- Gutowska, A.; Li, L.; Shin, Y.; Wang, C. M.; Li, X. S.; Linehan, J. C.; Smith, R. S.; Kay, B. D.; Schmid, B.; Shaw, W.; Gutowski, M.; Autrey, T. *Angew. Chem., Int. Ed.* **2005**, *44*, 3578.
- Stephens, F. H.; Pons, V.; Baker, R. T. *Dalton Trans.* **2007**, 2613.
- Marder, T. B. *Angew. Chem., Int. Ed.* **2007**, *46*, 8116.
- Xiong, Z. T.; Chua, Y. S.; Wu, G. T.; Xu, W. L.; Chen, P.; Shaw, W.; Karkamkar, A.; Linehan, J.; Smurthwaite, T.; Autrey, T. *Chem. Commun.* **2008**, 5595.
- Xiong, Z. T.; Yong, C. K.; Wu, G. T.; Chen, P.; Shaw, W.; Karkamkar, A.; Autrey, T.; Jones, M. O.; Johnson, S. R.; Edwards, P. P.; David, W. I. F. *Nat. Mater.* **2008**, *7*, 138.
- Wang, P.; Orimo, S.; Tanabe, K.; Fujii, H. *J. Alloys Compd.* **2003**, *350*, 218.
- Wu, H.; Zhou, W.; Yildirim, T. *J. Am. Chem. Soc.* **2008**, *130*, 14834.
- Wu, C.; Wu, G.; Xiong, Z.; David, W. I. F.; Ryan, K. R.; Jones, M. O.; Edwards, P. P.; Chu, H.; Chen, P. *Inorg. Chem.* **2010**, *49* (9), 4319.
- Luedtke, A. T.; Autrey, T. *Inorg. Chem.* **2010**, *49*, 3905.
- Xiong, Z. T.; Wu, G. T.; Chua, Y. S.; Hu, J. J.; He, T.; Xu, W. L.; Chen, P. *Energy Environ. Sci.* **2008**, *1*, 360.



- (12) Diyabalanage, H. V. K.; Shrestha, R. P.; Semelsberger, T. A.; Scott, B. L.; Bowden, M. E.; Davis, B. L.; Burrell, A. K. *Angew. Chem., Int. Ed.* **2007**, *46*, 8995.
- (13) Chua, Y. S.; Wu, G.; Xiong, Z.; He, T.; Chen, P. *Chem. Mater.* **2009**, *21*, 4899.
- (14) Chua, Y. S.; Wu, G.; Xiong, Z.; Karkamkar, A.; Guo, J.; Jian, M.; Wong, M. W.; Autrey, T.; Chen, P. *Chem. Commun.* **2010**, *46*, 5752.
- (15) Xia, G.; Yu, X.; Guo, Y.; Wu, Z.; Yang, C.; Liu, H.; Dou, S. *Chem.—Eur. J.* **2010**, *16*, 3763.
- (16) Chua, Y. S.; Wu, G.; Xiong, Z.; Karkamkar, A.; Guo, J.; Jian, M.; Wong, M. W.; Autrey, T.; Chen, P. *Chem. Commun.* **2010**, *46* (31), 5752.
- (17) Ramzan, M.; Silvearv, F.; Blomqvist, A.; Scheicher, R. H.; Lebegue, S.; Ahuja, R. *Phys. Rev. B* **2009**, *79*, 132102.
- (18) Kim, D. Y.; Singh, N. J.; Lee, H. M.; Kim, K. S. *Chem.—Eur. J.* **2009**, *15*, 5598.
- (19) Nutt, W. R.; McKee, M. L. *Inorg. Chem.* **2007**, *46*, 7633.
- (20) Kohn, W.; Sham, L. J. *Phys. Rev.* **1965**, *140*, A1133.
- (21) Blöchl, P. E. *Phys. Rev. B* **1994**, *50*, 17953.
- (22) Kresse, G.; Furthmüller, J. *Phys. Rev. B* **1996**, *54*, 11169.
- (23) Perdew, J. P.; Wang, Y. *Phys. Rev. B* **1992**, *45*, 13244.
- (24) Perdew, J. P.; Wang, Y. *Phys. Rev. B* **1992**, *45*, 13244.
- (25) Perdew, J. P.; Chevary, J. A.; Vosko, S. H.; Jackson, K. A.; Pederson, M. R.; Singh, D. J.; Fiolhais, C. *Phys. Rev. B* **1992**, *46*, 6671.
- (26) Wolverton, C.; et al. *J. Phys.: Condens. Matter* **2008**, *20*, 064228.
- (27) Siegel, D. J.; Wolverton, C.; Ozoliņš, V. *Phys. Rev. B* **2007**, *75*, 014101.
- (28) Ozoliņš, V.; et al. *J. Phys.: Conf. Ser.* **2009**, *180*, 012076.
- (29) Hector, L. G.; Herbst, J. F. *J. Phys.: Condens. Matter* **2008**, *20*, 064229.
- (30) Perdew, J. P.; Burke, K.; Ernzerhof, M. *Phys. Rev. Lett.* **1996**, *77*, 3865.
- (31) Spielmann, J.; Jansen, G.; Bandmann, H.; Harder, S. *Angew. Chem., Int. Ed.* **2008**, *47*, 6290.
- (32) Blöchl, P. E.; Jepsen, O.; Andersen, O. K. *Phys. Rev. B* **1994**, *49*, 16223.
- (33) Monkhorst, H. J.; Pack, J. D. *Phys. Rev. B* **1976**, *13*, 5188.
- (34) Kresse, G.; et al. *EPL (Europhysics Letters)* **1995**, *32*, 729.
- (35) Parlinski, K.; Li, Z. Q.; Kawazoe, Y. *Phys. Rev. Lett.* **1997**, *78*, 4063.
- (36) Togo, A. *Phonopy Program*; <http://phonopy.sourceforge.net/> (accessed March 2011).
- (37) Henkelman, G.; Uberuaga, B. P.; Jónsson, H. *J. Chem. Phys.* **2000**, *113*, 9901.
- (38) Li, C.-L.; et al. *Commun. Theor. Phys.* **2010**, *53*, 1167.
- (39) Nguyen, V. S.; Matus, M. H.; Grant, D. J.; Nguyen, M. T.; Dixon, D. A. *J. Phys. Chem. A* **2007**, *111*, 8844.
- (40) Shaw, W. J.; Linehan, J. C.; Szymczak, N. K.; Heldebrant, D. J.; Yonker, C.; Camaioni, D. M.; Baker, R. T.; Autrey, T. *Angew. Chem., Int. Ed.* **2008**, *47*, 7493.
- (41) Swinnen, S.; Nguyen, V. S.; Nguyen, M. T. *Chem. Phys. Lett.* **2010**, *489*, 148.
- (42) Lee, T. B.; McKee, M. L. *Inorg. Chem.* **2009**, *48*, 7564.
- (43) Yang, J.; Sudik, A.; Wolverton, C.; Siegel, D. J. *Chem. Soc. Rev.* **2010**, *39*, 656.
- (44) Yang, J.; Hirano, S. *Adv. Mater.* **2009**, *21*, 3023.
- (45) Araujo, C. M.; Scheicher, R. H.; Ahuja, R. *Appl. Phys. Lett.* **2008**, *92*, 021907.
- (46) Chase, M. W., Jr. *J. Phys. Chem. Ref. Data* **1998**, *Monograph* 9, 1.
- (47) West, D.; Limpijumnong, S.; Zhang, S. B. *Phys. Rev. B* **2009**, *80*, 064109.